Optical Engineering

SPIEDigitalLibrary.org/oe

One-dimensional gradient-index metrology based on ray slope measurements using a bootstrap algorithm

Di Lin
James R. Leger
Mint Kunkel
Peter McCarthy

Downloaded From: http://opticalengineering.spiedigitallibrary.org/ on 02/24/2014 Terms of Use: http://spiedl.org/terms

One-dimensional gradient-index metrology based on ray slope measurements using a bootstrap algorithm

Di Lin
James R. Leger
Mint Kunkel
University of Minnesota
Department of Electrical and Computer Engineering
Minneapolis, Minnesota 55455
E-mail: linx0284@gmail.com

Peter McCarthy
University of Rochester
Institute of Optics
Rochester, New York 14627-0186

Abstract. The refractive index profile of one-dimensional gradient-index (GRIN) samples can be measured using the incident and exit beam angles of multiple beams passing through the sample at different positions along the index gradient. Beginning from a region of known refractive index, the collective angular deflection measurement of multiple beams is bootstrapped to compute the index profile of the entire sample. An alternative method using an approximate beam displacement model and a corrective algorithm is also presented. The two techniques are used to measure the index profile of a thick GRIN sample, and experimental results show good agreement with a maximum discrepancy of 1.5×10^{-3} in the calculated index. An index accuracy of 5×10^{-4} is predicted for the bootstrap method employing typical micron-level spatial measurements. *© 2013 Society of Photo-Optical Instrumentation Engineers (SPIE)* [DOI: 10.1117/1.OE.52.11.112108]

Subject terms: deflectometry; metrology; gradient index; geometric optics.

Paper 130579SS received Apr. 15, 2013; revised manuscript received Jun. 14, 2013; accepted for publication Jun. 17, 2013; published online Jul. 16, 2013.

1 Introduction

Recent developments in the fabrication of gradient-index (GRIN) materials make it possible to create increasingly complex refractive index distributions. Several of these fabrication techniques are reported and discussed in Ref. 1. These GRIN materials are proving to be useful in a variety of applications. Fibers pulled from GRIN preforms can be designed to reduce modal dispersion and thereby increase the bandwidth and repeater distance of optical communication systems. Lenses made using GRIN profiles find application in telecommunications and compact imaging, where their small size and flat faces give them attractive packaging properties. GRIN elements can also be combined with conventional homogeneous glass elements to broaden the design space of imaging lenses. In particular, GRIN lens materials often have unique dispersion characteristics, making them useful for chromatic aberration correction.[2] Finally, in recent studies, GRIN materials have shown utility in coherent mode conversion and beam shaping applications.[3,4]

The integration of GRIN elements into an optical system requires an accurate knowledge of the optical properties of the inhomogeneous materials. The refractive index distribution of the GRIN element is of paramount importance because it determines the propagation behavior of light inside the medium. Conventional beam deflectometry methods use beam displacement[5,6] or beam angle[7] as a direct measurement of the index gradient. These methods are accurate only where the index gradient remains relatively constant across the beam trajectory inside the sample. When a significant amount of refraction occurs inside the sample, fundamental geometric assumptions in these methods become invalid and the measurements are difficult to interpret. Interferometric methods use fringe patterns to recover the phase profile of a beam propagating through the GRIN sample.[8] However, as the propagation distance through the sample becomes substantial, resolving fringes becomes impractical. In addition, ambiguity of the propagated phase profile can result from interferometric measurements without prior knowledge of the type of index variations present in the GRIN sample (e.g., diffusion-based GRIN elements may be restricted to regions of monotonic index variations based on the physics of diffusion). This makes interferometry unreliable for measuring arbitrary GRIN materials. Holographic methods have also been proposed that use multidirectional measurements of optical path length to recover the index distribution of GRIN samples.[9] However, the approximations made in these methods are not well suited to applications where a significant amount of refraction occurs inside the sample. In addition, data acquisition using holography can be very tedious. Older methods that do not have a practical automated process of data acquisition and have difficulties in accurate measurements when moderate index gradients are present include prism methods[10,11] and moiré patterns.[12,13]

In this paper, we propose a new measurement technique that is based on a very simple fundamental relation for one-dimensional (1-D) GRIN distributions[14] that does not have implicit restrictions on the magnitude of the index gradient. This method is appropriate for both longitudinal index gradients $n(y)$ and radial index gradients $n(r)$. We show a very straightforward method to acquire the necessary data and describe a procedure for its analysis. We contrast this with a second method that uses an iterative ray trace algorithm to correct for intrinsic errors in previous measurement procedures.

2 Ray Slope Measurements and the Bootstrap Algorithm

The bootstrap algorithm relies on a fundamental relation that follows directly from the ray equation in geometric optics.

$$\frac{d}{ds}\left(n\frac{d\vec{r}}{ds}\right) = \nabla n, \tag{1}$$

0091-3286/2013/$25.00 © 2013 SPIE

Downloaded From: http://opticalengineering.spiedigitallibrary.org/ on 02/24/2014 Terms of Use: http://spiedl.org/terms

where ds is the arc length along the ray path, $\vec{r}$ is the position vector of a point on the ray trajectory, and n is the refractive index. If the index is only allowed to vary along y, the refractive indices at two locations along a ray path are related by the slope of the ray at those locations[14] (see Appendix):

$$\frac{1+(y_1')^2}{1+(y_2')^2}=\frac{n(y_1)^2}{n(y_2)^2}, \tag{2}$$

where $y'=\frac{dy}{dx}$ denotes the slope of the ray at position y. If the locations are taken to be the ray path at the input and output surfaces outside the GRIN sample, then the application of Snell's law of refraction at those surfaces changes the relationship in Eq. (2) to

$$n(y_{\text{out}})^2=n(y_{\text{in}})^2+n_{\text{amb}}^2\left[\frac{(y_{\text{out}}')^2}{1+(y_{\text{out}}')^2}-\frac{(y_{\text{in}}')^2}{1+(y_{\text{in}}')^2}\right], \tag{3}$$

where n_{amb} is the refractive index of the ambient medium.[14] The quantities of interest are illustrated in Fig. 1.

Equation (3) is the fundamental relation for the bootstrap algorithm. The method requires a measurement of the probe beam's input and output positions as well as its input and output angles. It uses the index at the input end of the beam to calculate the index at the output end, or vice versa. Theoretically, it is possible to solve for the index distribution along a beam path that connects the input and output rays by inverting an integral equation relating the beam path and the refractive index distribution.[15] However, a solution to the inversion of the integral equation is not always guaranteed when measurement errors are present. In the bootstrap algorithm, only the refractive indices at the input and output locations of each ray path are pertinent. If the refractive index is known at some position y_0, then the index everywhere in the GRIN sample can be calculated using the relation in Eq. (3) if the input positions of all probe beams used in the measurement coincide with y_0, as illustrated in Fig. 2. In practice, however, the range of input angles for the probe beams is restricted by total internal reflection conditions. This limits the region of the GRIN sample that can be measured in convenient experimental setups.

The index is more typically known at the ends of the GRIN sample. In this case, angled incidence can be used to relate the fundamental expression in Eq. (3) for multiple ray paths (i.e., the trajectories of different probe beams) and the collective measurement can be bootstrapped to compute the index distribution across the entire sample. In this measurement geometry, as shown in Fig. 3, the incident beam is angled to ensure there are always rays traveling from a known region of the GRIN profile to the unknown region (or vice versa).

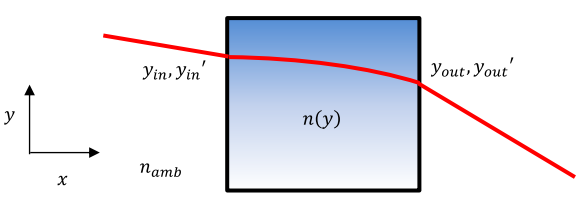

Fig. 1 Illustrating the fundamental relation in Eq. (3).

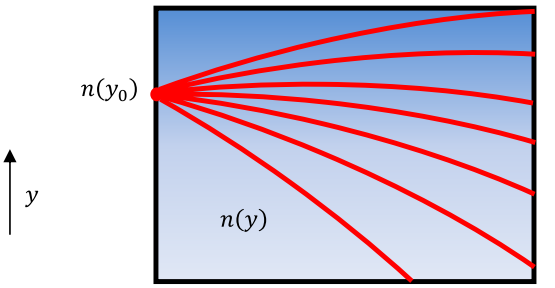

Fig. 2 Measuring refractive index of a GRIN sample from a known value at position y_0.

The expansion of the known region of the GRIN profile can be readily seen in Fig. 3, where the initially known region of the sample is below the green dashed line. The ray farthest from the known region that can be used to calculate the index in the initially unknown region has output position y_1. With the help of Eq. (3), index values can be calculated up to y_3 and all values for $y < y_3$ can be interpolated from known or calculated values. This expands the known region up to y_3, allowing the output ray at y_2 to be used in a subsequent calculation. This process is defined as one bootstrap in the algorithm, i.e., the process of expanding the calculated index profile of the sample by applying Eq. (3) to all applicable rays. Each bootstrap will yield new information about the sample until all rays from the measurement have been exhausted and the entire index distribution has been computed. It is important to bear in mind that the bootstrap process can terminate early if the incident angle is too shallow and ray trajectories are bent aggressively toward the unknown region by steep index gradients. In general, choosing the appropriate angle of incidence and a sufficient number of probe beams is enough to guarantee the completion of the algorithm.

3 Finite Beam Width Effects and Beam Shaping

Index gradients in inhomogeneous transparent materials are able to manipulate the propagation of light rays inside the medium, distorting the irradiance profile of an optical beam passing through the sample. If the beam is narrow relative to the index gradient, the distortion to its irradiance profile is negligible and the beam behaves like an ideal light ray (assuming diffraction can be ignored). However, a significant change in the index gradient across the transverse profile of the optical beam will cause a redistribution of the beam's irradiance. This beam shaping effect can yield additional information about the index distribution in question.

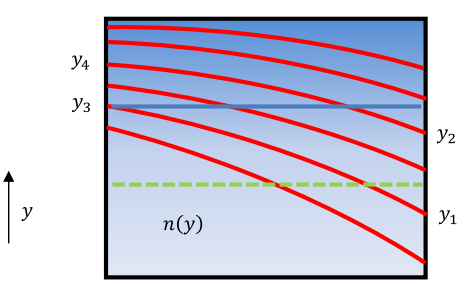

Fig. 3 Angled incidence for bootstrapping refractive index calculations.

Downloaded From: http://opticalengineering.spiedigitallibrary.org/ on 02/24/2014 Terms of Use: http://spiedl.org/terms

Energy conservation allows for a correspondence between the field description of an optical beam and an equivalent ray distribution[2] when diffraction effects are negligible. Upon establishing this relationship, beam shaping in inhomogeneous media can be treated as a distributed version of beam deflection. An important question to ask is how the propagation behavior of a finite-sized optical beam in an inhomogeneous medium matches the behavior of the desired ideal ray. In experimental measurements involving finite-sized probe beams, the median of the beam irradiance profile can be used as an estimate of the location of the ideal ray. In the limit of infinitesimally small beam width, the ideal ray must follow a path dictated by Eq. (1). As the beam size increases, it can be shown through energy conservation that if the individual paths of the rays contained in the optical beam do not intersect with the ideal ray, the ideal ray path will always coincide with the median of the optical beam, as can be seen in Fig. 4.

If all rays in Fig. 4 carry the same amount of radiative flux, then the total integrated flux on either side of the ideal ray (dashed red) is constant between the two planes and the location of the median must follow the path of the ideal ray. Thus, a location of a single ray can be effectively measured with a finite-sized beam by using the median of the beam intensity under these circumstances. This is particularly useful for experimental measurements.

Since beam shaping effects can be treated as a distributed version of beam deflection, it is possible to obtain all the beam deflection data required for the deflectometry measurement using a single optical beam of sufficient width. By measuring the irradiance profiles in two observation planes outside the sample and applying energy conservation, a ray distribution (specifying both angles and positions) can be extrapolated for any plane outside the sample. An advantage of using a simple beam shaping measurement with a wide beam is that only a single measurement is needed. The caveat is that because energy conservation is only applied at the observation planes where the beam's irradiance profile is measured, it is assumed that the individual rays do not intersect with each other between observation planes. This condition imposes a constraint on the geometry of the experiment. However, the primary issue for this type of measurement is the presence of coherent noise in the system. Due to the nature of this calculation, noisy irradiance profiles can introduce a significant shift in the constituent ray positions at the observation planes. The uncertainty in calculated ray positions due to coherent noise is typically much greater than the uncertainty in conventional beam deflection measurements.

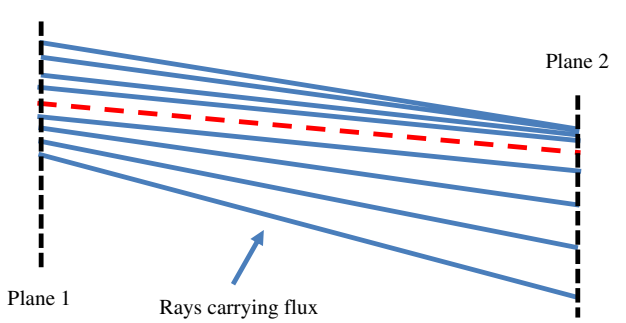

Fig. 4 An ideal ray (dashed red) tracking the median of an optical beam's irradiance profile.

4 Beam Deflectometry Based on Ray Position

In order to assess the performance of our proposed method, we have compared it to previous methods of beam deflectometry based on measuring the entering and exiting ray positions rather than the ray angles.[5] These methods contain inherent approximations and are thus expected to be less accurate than the one proposed in Sec. 2. In addition, the method described in Ref. 5 requires normal incidence on one surface of the GRIN sample in order to reduce the complexity of the measurement.

The method is briefly described in Fig. 5. If a circular ray path is assumed inside the GRIN material and small-angle approximations are taken, the displacement of a beam in a distant plane from its initial position is

$$\frac{\partial n}{\partial y} \approx \frac{\Delta}{LD}, \tag{4}$$

where D is the propagation distance from the sample exit surface to the distant plane and L is the thickness of the sample. The measured deflection data over the sample, $\Delta(y)$, can then be integrated to arrive at the relative index distribution. The assumptions and approximations made in this method allow for the displacement of the beam to be measured in one plane, rather than two planes, as required in the bootstrap method to measure angular deflection of the beam. However, the approximations in this method ultimately limit the accuracy of the measurement.

In order to improve the measurement accuracy of this method, an iterative ray trace correction algorithm was developed using the result of Eq. (4) as a starting point. An error metric is defined as the root-mean-squared (RMS) difference between the measured deflection data and calculated deflection data using forward ray tracing through the GRIN sample, including free-space propagation to the observation plane. The GRIN profile is parameterized such that an optimization can be performed over the GRIN parameters to minimize the error metric. Any appropriate parameterization can be used, but cubic splines offer a practical and flexible parameter space. The locations of the spline knots are optimized until the resulting index profile produces ray trace deflection data that are consistent with the measured data. An inherent advantage of this type of approach is that additional sample parameters that affect measurement accuracy, such as wedge and surface shape, can be accounted for in the forward ray trace (so long as they can be measured.)

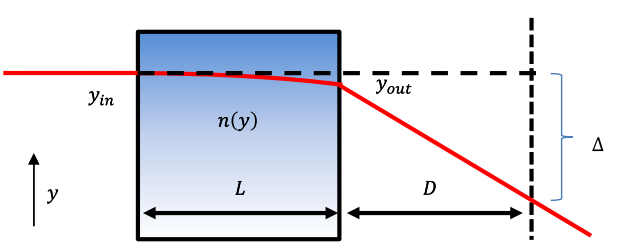

Fig. 5 Deflectometry geometry in the ray displacement method.

Downloaded From: http://opticalengineering.spiedigitallibrary.org/ on 02/24/2014 Terms of Use: http://spiedl.org/terms

5 Experimental Measurement

The foregoing theoretical discussion suggests two GRIN metrology techniques: a ray slope method using a bootstrap algorithm (described in Sec. 2) and a ray position method (described in Sec. 4) using an iterative correction algorithm. The ray slope method, based on Eq. (3), requires beam position and angle measurements at the input and output surfaces of the GRIN sample. These quantities are obtained using a relatively straightforward benchtop setup, illustrated in Fig. 6. The position of the beam at the output surface of the sample is extrapolated from beam position measurements in two observation planes. In the ray position method, the geometry is simpler, where the probe beam is normally incident and beam position is only measured in one observation plane behind the GRIN sample (as seen in Fig. 5).

The calculated index profiles obtained from the two measurement techniques described in the preceding sections, as well as the discrepancy between them, are shown in Fig. 7. The sample used was a polymer blend of polymethyl methacrylate and polystyrene produced at the University of Rochester with a thickness of 14.03 mm. The two calculated profiles are in good agreement, but it cannot be determined which of the two methods is more accurate since the actual index profile of the sample is unknown. Given the uncertainty in position measurements, it is possible to obtain an error bound (as well as the expected error) for the calculated index distribution. The error analysis for both methods is deferred to a later section. The maximum discrepancy between the index distributions calculated from both methods in this particular measurement is 1.5×10^{-3}. This is reasonable considering the uncertainty in position measurements and a relatively short propagation distance (2.2 cm) between the output face of the sample and the farthest observation plane. To improve measurement accuracy in the ray slope method, the propagation distance between observation plane 1 and the sample should be minimized while extending the propagation distance to observation plane 2. Similarly, increasing the propagation distance between the sample and the observation plane will reduce error buildup in the ray position method.

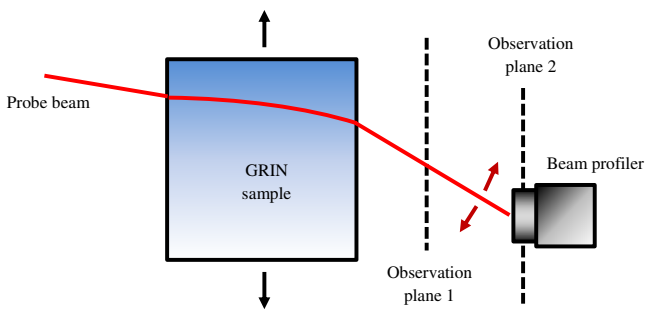

Fig. 6 Experimental setup for measuring 1-D gradient index (GRIN) profiles using angled incidence.

6 Intrinsic Error Analysis

6.1 *Ray Position Method*

The ray displacement method described in Sec. 4 uses first-order small-angle approximations along with other simplifying assumptions. When beam displacement inside the GRIN sample becomes significant, these assumptions break down and a substantial error can result in the calculated index. The following analysis provides a second-order correction term to the small-angle approximation and addresses finite beam deflection taking place inside the sample. The difference between the geometry of beam deflection and its approximated model is illustrated in Fig. 8.

Retaining the second-order terms in the small-angle approximations, one finds that

$$\Delta_{\mathrm{GRIN}} = R[1-\cos(\theta_1)] \approx \frac{n}{\frac{\partial n}{\partial y}}\frac{1}{2}\theta_1^2. \tag{5}$$

Consequently, the first-order expression in Eq. (4) becomes (following a similar derivation used in Ref. 5)

$$\frac{\partial n}{\partial y} = \frac{\Delta_{\mathrm{tot}}}{LD + \frac{L^2}{2n}}, \tag{6}$$

where $\Delta_{\mathrm{tot}} = \Delta_{\mathrm{GRIN}} + \Delta_{\mathrm{ext}}$ is the total beam displacement. Equation (6) provides a more accurate description (second order) of the index profile, especially in thicker samples or where the index distributions contain significant gradients. A forward ray trace (simulation) is performed for normally incident beams propagating through a GRIN sample with an index distribution shown in Fig. 9(a). The sample thickness is 0.3 cm and the measurement plane is placed 0.5 cm away from the output surface of the sample. These

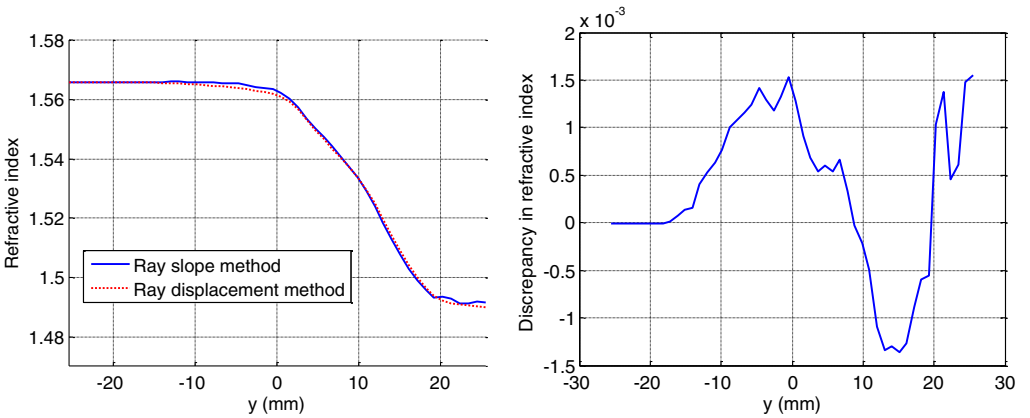

Fig. 7 Comparison between index profiles measured using the ray slope method and the ray displacement method.

Downloaded From: http://opticalengineering.spiedigitallibrary.org/ on 02/24/2014 Terms of Use: http://spiedl.org/terms

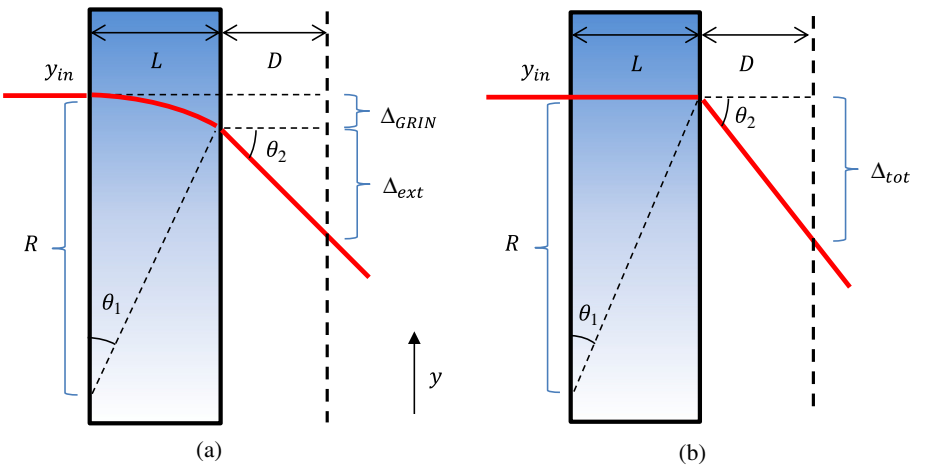

Fig. 8 Difference between (a) beam deflection geometry and (b) first-order small-angle model.

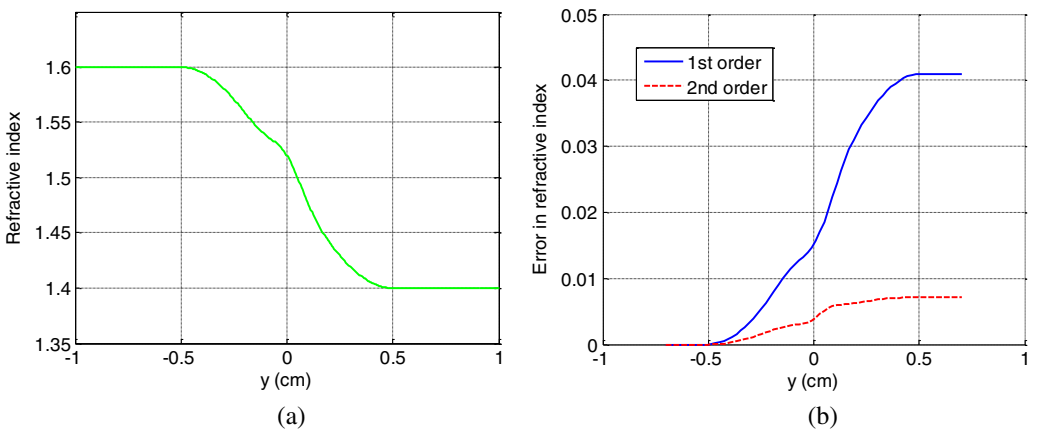

Fig. 9 (a) Index profile used in simulation to generate beam displacement data. (b) Intrinsic errors in index values resulting from first- and second-order approximations. Simulation parameters are set to $L = 0.3$ cm and $D = 0.5$ cm.

simulation parameters were chosen such that substantial error in the index would result from approximations made in the ray position method of Sec. 4. The improvement in the computation error after applying Eq. (6) can be seen in Fig. 9(b).

It is clear that even a second-order small-angle approximation will not suffice under these conditions. Fundamental assumptions in the approximate model also break down under similar circumstances. In particular, the actual ray trajectory will deviate from the assumed circular arc under a constant index gradient, as shown in Fig. 10. The circular arc remains a relatively good approximation in thicker samples compared to the more commonly used parabolic ray path in small-angle approximations. However, any assumed ray path under a constant index gradient becomes problematic in thick samples because the index gradient generally does not remain constant across the ray path.

These intrinsic errors are corrected by the iterative ray trace algorithm following the initial calculation from Eq. (6) [in lieu of Eq. (4) for faster convergence]. The result is shown in Fig. 11. The remaining error primarily originates from quantization and parameterization effects in the forward ray trace used to generate the beam deflection data and is not a limitation to the accuracy that can be achieved by the algorithm.

6.2 *Ray Slope Method*

A similar simulation is performed for the same GRIN profile shown in Fig. 9(a) using the ray slope method. Beam deflection data are generated from a forward ray trace for probe beams incident at $\theta = \pi/7$ rad. The index calculated from the bootstrap algorithm and the resulting error is shown in

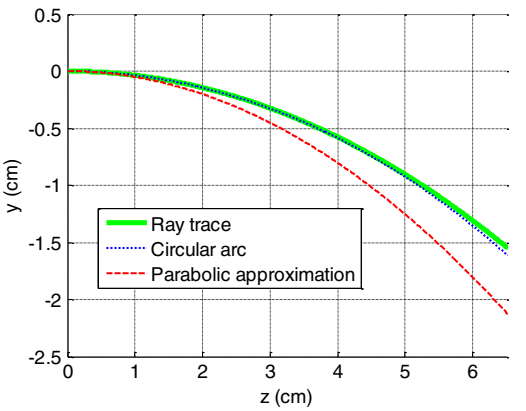

Fig. 10 Intrinsic error in the ray path assumed in the ray position method under a constant index gradient of 0.1 cm^{-1}.

Downloaded From: http://opticalengineering.spiedigitallibrary.org/ on 02/24/2014 Terms of Use: http://spiedl.org/terms

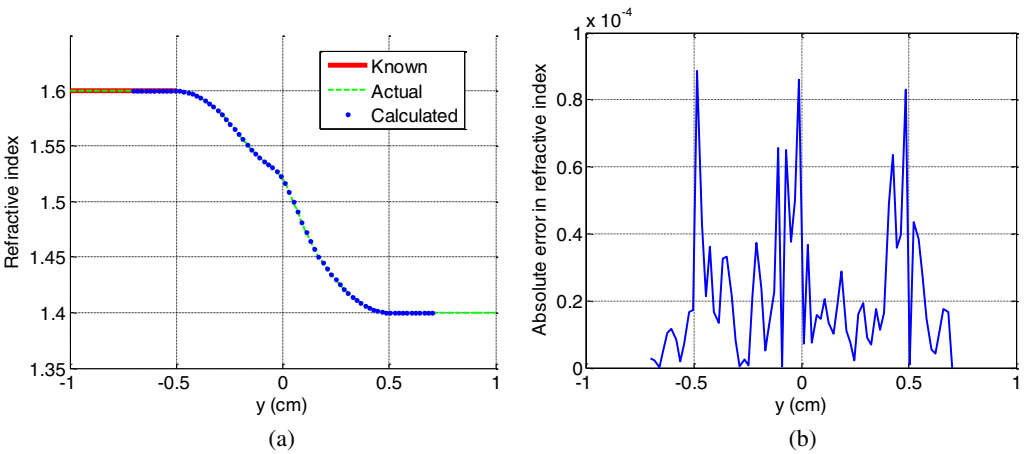

Fig. 11 (a) Index calculated from the ray displacement method using the iterative ray trace correction algorithm. The curves for actual and calculated results cannot be discerned from this plot. (b) The resulting error due to quantization effects in the simulation. Simulation parameters are unchanged from Fig. 9.

Fig. 12. We hasten to add this error does not represent a fundamental limit on the accuracy of the bootstrap algorithm. Since no approximations were used in the derivation of the fundamental relation in Eq. (3), any intrinsic (nonmeasurement-based) error in the ray slope method is due simply to the accuracy of the interpolator used in the bootstrap algorithm.

7 Measurement Error Analysis

In this section, we examine the effects of measurement error on both methods. Error propagation is of particular concern since calculated index values are used in subsequent calculations in the bootstrap algorithm and integration over calculated gradients is used to find the index distribution in the ray displacement method.

In order to quantify the accumulation of error from the bootstrap process, sources of measurement error need to be identified. Starting with the fundamental relation from Eq. (3) and assuming the probe beams are traveling from an unknown region at the input to a known region of the sample at the output, the refractive index at the input can be calculated as

$$n_{\text{in}} = \left[n_{\text{out}}^2 - \frac{n_{\text{amb}}^2 (y'_{\text{out}})^2}{1 + (y'_{\text{out}})^2} + \frac{n_{\text{amb}}^2 (y'_{\text{in}})^2}{1 + (y'_{\text{in}})^2} \right]^{\frac{1}{2}}, \tag{7}$$

where the refractive index at the output, $n_{\text{out}} = n(y_{\text{out}})$, is a known (or calculated) quantity and the slopes, y'_{out} and y'_{in}, are measured quantities. Differentiating n_{in} with respect to these quantities yields

$$\frac{\partial n_{\text{in}}}{\partial n_{\text{out}}} = n_{\text{out}} \left[n_{\text{out}}^2 - \frac{n_{\text{amb}}^2 (y'_{\text{out}})^2}{1 + (y'_{\text{out}})^2} + \frac{n_{\text{amb}}^2 (y'_{\text{in}})^2}{1 + (y'_{\text{in}})^2} \right]^{-\frac{1}{2}}, \tag{8}$$

$$\frac{\partial n_{\text{in}}}{\partial (y'_{\text{out}})} = \left[- \frac{n_{\text{amb}}^2 (y'_{\text{out}})}{1 + 2(y'_{\text{out}})^2 + (y'_{\text{out}})^4} \right] \times \left[n_{\text{out}}^2 - \frac{n_{\text{amb}}^2 (y'_{\text{out}})^2}{1 + (y'_{\text{out}})^2} + \frac{n_{\text{amb}}^2 (y'_{\text{in}})^2}{1 + (y'_{\text{in}})^2} \right]^{-\frac{1}{2}}, \tag{9}$$

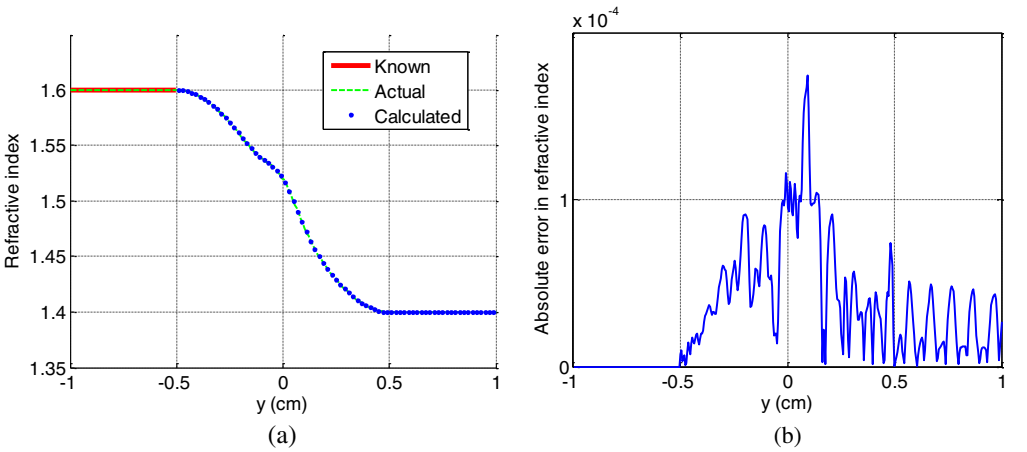

Fig. 12 (a) Index calculated from the ray slope method using the bootstrap algorithm. The curves for actual and calculated results cannot be discerned from this plot. (b) The resulting error due to quantization effects in the simulation. Simulation parameters are set to $L = 0.3$ cm and $a = b = 0.25$ cm.

Downloaded From: http://opticalengineering.spiedigitallibrary.org/ on 02/24/2014 Terms of Use: http://spiedl.org/terms

$$\frac{\partial n_{\text{in}}}{\partial(y'_{\text{in}})} = \left[\frac{n^2_{\text{amb}}(y'_{\text{in}})}{1+2(y'_{\text{in}})^2+(y'_{\text{in}})^4}\right] \times \left[n^2_{\text{out}} - \frac{n^2_{\text{amb}}(y'_{\text{out}})^2}{1+(y'_{\text{out}})^2} + \frac{n^2_{\text{amb}}(y'_{\text{in}})^2}{1+(y'_{\text{in}})^2}\right]^{-\frac{1}{2}}. \quad (10)$$

The total error when calculating the index in the input plane is therefore

$$dn_{\text{in}} = \frac{\partial n_{\text{in}}}{\partial n_{\text{out}}} dn_{\text{out}} + \frac{\partial n_{\text{in}}}{\partial(y'_{\text{out}})} d(y'_{\text{out}}) + \frac{\partial n_{\text{in}}}{\partial(y'_{\text{in}})} d(y'_{\text{in}}). \quad (11)$$

The geometry of the beam deflection measurement is illustrated in Fig. 13. The angles in Eq. (11) are obtained by measuring the beam position in two observation planes. Computational error can result from uncertainty in the position measurements of the probe beam in the observation planes as well as uncertainty in the positions of the observation planes themselves.

Rewriting Eq. (11) in terms of the measured quantities a, b, y_a, and y_b, the total accumulated error bound is given by (see Appendix):

$$\begin{aligned} dn_{\text{in}} = &\left[-\frac{\partial n_{\text{in}}}{\partial n_{\text{out}}}\frac{\partial n}{\partial y}\left(1+\frac{a}{b}\right) - \frac{\partial n_{\text{in}}}{\partial(y'_{\text{out}})}\frac{1}{b}\right] dy_a \\ &+ \left[\frac{\partial n_{\text{in}}}{\partial n_{\text{out}}}\frac{\partial n}{\partial y}\frac{a}{b} + \frac{\partial n_{\text{in}}}{\partial(y'_{\text{out}})}\frac{1}{b}\right] dy_b \\ &+ \frac{\partial n_{\text{in}}}{\partial n_{\text{out}}}\frac{\partial n}{\partial y}(y'_{\text{out}})da \\ &+ \left[-\frac{\partial n_{\text{in}}}{\partial n_{\text{out}}}\frac{\partial n}{\partial y}\frac{a}{b}(y'_{\text{out}}) - \frac{\partial n_{\text{in}}}{\partial(y'_{\text{out}})}\frac{1}{b}(y'_{\text{out}})\right] db \\ &+ + \frac{\partial n_{\text{in}}}{\partial(y'_{\text{in}})} d(y'_{\text{in}}) + \frac{\partial n_{\text{in}}}{\partial n_{\text{out}}}(dn_{\text{interp}} + dn^*_{\text{in}}), \end{aligned} \quad (12)$$

where dn_{interp} is the interpolation error, dn^*_{in} accounts for the accumulated error in the calculated index profile from previous bootstraps as well as error in the measured input beam position (see Appendix), and partial derivatives involving n_{out}, y'_{in}, and y'_{out} are given by Eqs. (8)–(10). By iteratively applying Eq. (12) N times, where N is the minimum number of bootstraps required to calculate the entire index profile of the sample, a bound on the accumulated error can be computed for the bootstrap algorithm. The error compounds with each bootstrap in the algorithm. If $|\frac{\partial n_{\text{in}}}{\partial n_{\text{out}}}| = 1$, the accumulated error bound will increase linearly with each bootstrap. From Eq. (8), this condition is satisfied when $|y'_{\text{in}}| = |y'_{\text{out}}|$ (always true in homogeneous samples). If $|y'_{\text{in}}| < |y'_{\text{out}}|$, it is clear that $|\frac{\partial n_{\text{in}}}{\partial n_{\text{out}}}| > 1$ and the maximum accumulated error increases exponentially per bootstrap. On the other hand, if $|y'_{\text{in}}| > |y'_{\text{out}}|$, then $|\frac{\partial n_{\text{in}}}{\partial n_{\text{out}}}| < 1$ and the accumulated error bound approaches an asymptote. One can take advantage of this particular type of buildup behavior in computation error when measuring samples with a monotonic index profile.

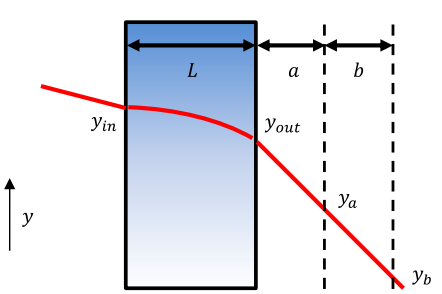

Fig. 13 Deflectometry geometry in the ray slope method.

While systematic errors result from uncertainty in propagation distances, a and b, uncertainty in position measurements, y_a and y_b, need to be treated as random processes. Using Eq. (12), the expected error resulting from these random variables in the two observation planes is given by

$$\begin{aligned} \Delta n^2_{\text{in,rms}} = &\left|-\frac{\partial n_{\text{in}}}{\partial n_{\text{out}}}\frac{\partial n}{\partial y}\left(1+\frac{a}{b}\right) - \frac{\partial n_{\text{in}}}{\partial(y'_{\text{out}})}\frac{1}{b}\right|^2 \Delta y^2_{a,\text{rms}} \\ &+ \left|\frac{\partial n_{\text{in}}}{\partial n_{\text{out}}}\frac{\partial n}{\partial y}\frac{a}{b} + \frac{\partial n_{\text{in}}}{\partial(y'_{\text{out}})}\frac{1}{b}\right|^2 \Delta y^2_{b,\text{rms}} \\ &+ \left|\frac{\partial n_{\text{in}}}{\partial(y'_{\text{in}})}\right|^2 \Delta(y'_{\text{in}})^2_{\text{rms}} \\ &+ \left|\frac{\partial n_{\text{in}}}{\partial n_{\text{out}}}\frac{\partial n}{\partial y}\frac{a}{b} + \frac{\partial n_{\text{in}}}{\partial(y'_{\text{out}})}\frac{1}{b}\right|^2 \Delta y^2_{b,\text{rms}} \\ &+ \left|\frac{\partial n_{\text{in}}}{\partial(y'_{\text{in}})}\right|^2 \Delta(y'_{\text{in}})^2_{\text{rms}} \\ &+ \left|\frac{\partial n_{\text{in}}}{\partial n_{\text{out}}}\right|^2 (\Delta n^2_{\text{interp,rms}} + \Delta n^{*2}_{\text{in,rms}}). \end{aligned} \quad (13)$$

To verify our error analysis, a forward ray trace is computed for a set of incident beams through a predetermined GRIN profile. A constrained cubic spline fit is used to interpolate between known (or calculated) index values. Therefore, noise from the interpolator is roughly fourth-order in the separation between output ray positions and can be neglected if a sufficiently large number of rays are used. However, because the output ray positions and angles are computed from a numerical ray trace and a discretized index profile, quantization noise must be considered. This noise term replaces the interpolation noise term in Eq. (12). For the purposes of verifying the error bound in Eq. (12), the bound on quantization noise in the calculated index profile was characterized to be roughly 2×10^{-5} (before the error compounds) for the resolution used in the simulation. Following the forward ray trace, position measurements, y_a and y_b, in the observation planes are uniformly shifted by 1 μm to introduce a systematic error. A similar perturbation can be achieved by changing propagation distances a and b in Fig. 13 after beam deflection data have been obtained. The accumulated error in the bootstrap algorithm due to this systematic error in output beam positions and angles is shown in Fig. 14(a). The results are in good agreement with the error bound predicted by Eq. (12). The discrepancy at larger y-values is because Eq. (12) assumes the error in each bootstrap always reaches the predicted error bound. This is only true for the first couple bootstraps in this particular simulation, as evident from Fig. 14(a). If the errors are random variations in position measurements, y_a and y_b, the accumulated error in the bootstrap algorithm will typically resemble Fig. 14(b). Taking the statistical average over a large number of realizations after

Downloaded From: http://opticalengineering.spiedigitallibrary.org/ on 02/24/2014 Terms of Use: http://spiedl.org/terms

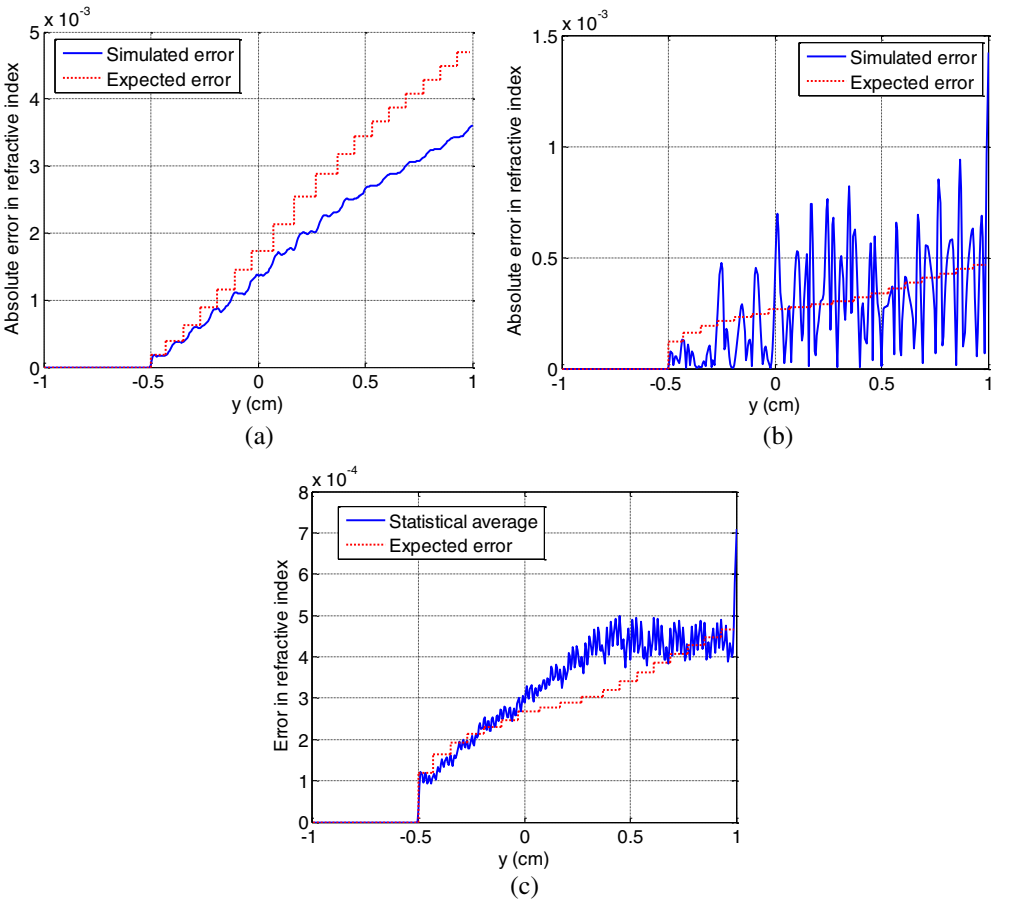

Fig. 14 (a) Accumulated error in the calculated index due to systematic errors in a single simulation. (b) Effect of random measurement errors in a single simulation. (c) The accumulated error due to random measurement errors is averaged (root mean squared [RMS]) over a large number of realizations (simulations) to determine the expected error. Simulation parameters are unchanged from Fig. 12.

adding normally distributed random noise with a standard deviation of 1 μm to the position measurements, the expected error conforms to Eq. (13), as shown in Fig. 14(c). The discrepancy arises because partial derivatives and the index gradient appearing in Eq. (13) are estimated in the bootstrap process when the index distribution is still unknown. Updating the accumulated error once per bootstrap in the algorithm results in the apparent staircase behavior in all three figures. In these simulations, multiple values of the index are calculated per bootstrap.

Since no analytical expression exists for the error produced by the iterative algorithm when there is uncertainty in spatial measurements, its performance is analyzed by adding normally distributed random noise with a standard deviation of 1 μm to the displacement data generated from a forward ray trace. A large number of simulations are averaged (RMS) to quantify the effect of these random errors. In addition, systematic errors are simulated by adding a constant 1-μm shift to all displacement data. The results of the analysis are shown in Fig. 15. Because beam displacement is a direct measure of the index gradient in the ray position method, error buildup due to systematic errors is expected to increase linearly with distance from the initially known region of the sample.

Compared to the ray slope method where ray displacement is measured in two planes to obtain slope data, the computation error is smaller in the ray position method due to a simpler measurement geometry. However, the numerical integration involved in computing the index distribution makes the displacement method more sensitive to the number of beams used in measuring the sample (since individual measurements correspond to the index gradient in the vicinity of the beam path), as well as the parameterization of the

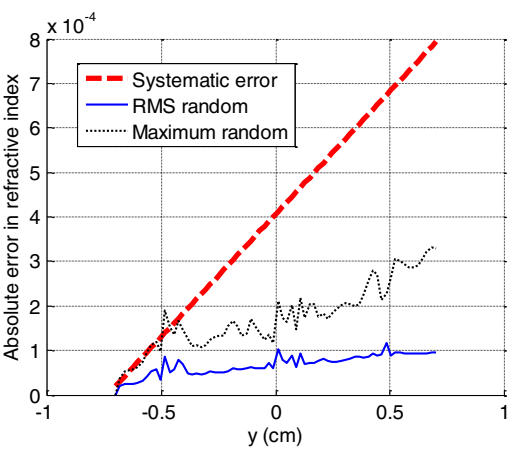

Fig. 15 Refractive index error in the ray trace correction algorithm due to systematic errors and random errors in simulated beam displacement data. Random errors are averaged (RMS) over a large number of realizations (simulations) to calculate the expected error. Simulation parameters are unchanged from Fig. 9.

Downloaded From: http://opticalengineering.spiedigitallibrary.org/ on 02/24/2014 Terms of Use: http://spiedl.org/terms

index profile for optimization. This also leads to error buildup in the calculated index at locations far from the initially known region of the sample. In contrast, the ray slope method is more robust in this regard; the error due to sparse data points only depends on the quality of the interpolator used in the bootstrap algorithm.

Redundancy in measured data provides one method of reducing error buildup in both methods. As currently presented, both methods use a known index value at one end of the sample as a starting point. With uncertainties in spatial measurements, index values calculated farther away from the known region generally contain more error. If the refractive index is known at both ends of the sample (or, in general, at multiple sample positions), the computation in both algorithms can be repeated, without any additional measurements, starting at these known points. Consistency among the index distributions obtained from different starting locations can be enforced to improve accuracy and mitigate error buildup in both algorithms.

Finally, it is worth mentioning that measurements from the ray slope method provide enough information to engage the previously described iterative ray trace algorithm after obtaining an initial index distribution via the bootstrap algorithm. However, much of the correction made in the ray trace algorithm comes from intrinsic modeling errors of the ray displacement method. Without measurement errors, the ray trace algorithm would work primarily to increase the interpolation accuracy of the bootstrap algorithm. If uncertainties are present in the measurements, combining the two algorithms would not necessarily lead to an improvement in the calculated index distribution, as the errors generated by the algorithms accumulate differently.

8 Conclusion

We have presented a new method for measuring 1-D index profiles using angular ray deflection measurements and compared it to an existing technique using ray position measurements. The new method uses a fundamental relation between input and output beam angles that follows directly from the ray equation in geometric optics and contains no approximations (apart from those necessary for neglecting diffraction). A bootstrap algorithm was introduced to compute the index distribution based on ray angle (and position) measurements. The accuracy of the existing ray position method was enhanced significantly by utilizing an iterative ray trace algorithm to correct for intrinsic errors incurred from using an approximate beam displacement model. Both methods were used to experimentally measure the index distribution of a 1-D GRIN sample. The results showed good agreement, with a maximum discrepancy of 1.5×10^{-3} in the calculated index between the two methods. In addition, we obtained an analytical expression for estimating error buildup in the bootstrap algorithm applied to the ray angle approach and verified the expression with a computer simulation. In a typical simulation, we expect the error buildup in the calculated index to be $<1 \times 10^{-3}$ for the ray angle approach. We have also simulated the effects of similar uncertainties in measurement of the calculated index distribution for the ray displacement method where an iterative ray trace algorithm was used to correct for the intrinsic modeling errors. Index of refraction measurements from both approaches show similar precision when similar measurement geometries and intrinsic measurement accuracies are assumed.

Acknowledgments

We gratefully acknowledge the contributions and valuable insight of Jeremy Teichman from the Institute for Defense Analyses, whose original suggestion to use ray slopes for refractive index measurements formed the basis of our method.

Appendix

The deduction of Eq. (2) from Eq. (1) is as follows. The first and second derivatives with respect to s in terms of Cartesian coordinates x and y can be written as

$$\frac{d}{ds} = \frac{d}{dx}\frac{dx}{ds} = \frac{d}{dx}\frac{dx}{\sqrt{dx^2 + dy^2}} = \frac{d}{dx}\frac{1}{\sqrt{1 + \left(\frac{dy}{dx}\right)^2}},$$

$$\frac{d^2}{ds^2} = \frac{d^2}{dx^2}\frac{1}{1 + \left(\frac{dy}{dx}\right)^2}$$

using the fact that $ds^2 = dx^2 + dy^2$. In scalar form, Eq. (1) can be rewritten as

$$\frac{dn}{dx}\left(\frac{dx}{ds}\right)^2 = \frac{\partial n}{\partial x}$$

$$\frac{dn}{dx}\frac{dx}{ds}\frac{dy}{ds} + n\frac{d^2y}{dx^2}\frac{1}{1 + \left(\frac{dy}{dx}\right)^2} = \frac{\partial n}{\partial y}.$$

Since the index only varies along y, $\frac{dn}{dx} = 0$ and the expressions above are reduced to

$$n\frac{d^2y}{dx^2}\frac{1}{1 + \left(\frac{dy}{dx}\right)^2} = \frac{\partial n}{\partial y}.$$

Multiplying both sides by $\frac{dy}{dx}$ and rearranging yields

$$\frac{d\left\{\ln\left[1 + \left(\frac{dy}{dx}\right)^2\right]\right\}}{dx} = \frac{d[2\ \ln(n)]}{dx}.$$

Integrating and applying the appropriate boundary condition produces the fundamental relation in Eq. (2).

Equation (12) can be deduced from Eq. (11) using the measured quantities shown in Fig. 13. The error in the calculated output slope is given by

$$d(y'_{\text{out}}) = \frac{1}{b}(dy_b - dy_a - y'_{\text{out}}db).$$

The error in position measurements produces an error in the known index at the output as a result of an uncertainty in the extrapolated output position y_{out},

$$dn_{\text{out}} = \frac{\partial n}{\partial y}dy_{\text{out}},$$

Downloaded From: http://opticalengineering.spiedigitallibrary.org/ on 02/24/2014 Terms of Use: http://spiedl.org/terms

where $\frac{\partial n}{\partial y}$ is the gradient of the index profile at y_{out} and the error in the extrapolated output position of the beam is given by

$$dy_{\text{out}} = \left(1 + \frac{a}{b}\right) dy_a - \frac{a}{b} dy_b - y'_{\text{out}} da + \frac{a}{b} y'_{\text{out}} db.$$

In the bootstrap algorithm, indices at the output are interpolated from previously calculated values. If the index at the output does not reside in the initially known region of the sample and was obtained from Eq. (3), then the total error in the calculated index at the output must account for interpolation error as well as any computation error carried over from previous calculations.

$$dn_{\text{out}} = \frac{\partial n}{\partial y} dy_{\text{out}} + dn_{\text{interp}} + dn^*_{\text{in}},$$

where dn_{interp} is the interpolation error and dn^*_{in} is the accumulated error in the GRIN profile from previous bootstraps with an additional term that accounts for spatial measurement errors in the input plane.

$$dn^*_{\text{in}} = dn_{\text{in,prev}} - \frac{\partial n}{\partial y} dy_{\text{in,prev}}.$$

Substituting the above expressions into Eq. (11) and rearranging yields the expression in Eq. (12). In Eq. (13), the accumulated RMS error appears in the form

$$\Delta n^{*2}_{\text{in,rms}} = \Delta n^2_{\text{in,rms,prev}} + \left|\frac{\partial n}{\partial y}\right|^2 \Delta y^2_{\text{in,rms}}.$$

References

1. D. T. Moore, "Gradient-index optics: a review," *Appl. Opt.* **19**(7), 1035–1038 (1980).
2. P. J. Sands, "Inhomogeneous lenses, V. Chromatic paraxial aberrations of lenses with axial or cylindrical index distributions," *J. Opt. Soc. Am.* **61**(11), 1495–1500 (1971).
3. C. Wang and D. L. Shealy, "Design of gradient-index lens systems for laser beam reshaping," *Appl. Opt.* **32**(25), 4763–4769 (1993).
4. D. Lin and J. R. Leger, "Numerical gradient-index design for coherent mode conversion," *Adv. Opt. Technol.* **1**(3), 195–202 (2012).
5. A. J. Barnard and B. Ahlborn, "Measurement of refractive index gradients by deflection of a laser beam," *Am. J. Phys.* **43**(7), 573 (1975).
6. O. Wiener, "Darstellung gekrummter Lichtstrahlen und Verwerthung derselben zur Untersuchung von Diffusion und Warmeleitung," *Ann. Phys. Chem.* **285**(5), 105–149 (1893).
7. Z. Bodnar and F. Ratajczyk, "Some remarks concerning optical glass heterogeneity measurement with the help of the autocollimation method," *Appl. Opt.* **4**(3), 351–354 (1965).
8. D. T. Moore and D. P. Ryan, "Measurement of the optical properties of gradient index materials," *J. Opt. Soc. Am.* **68**(9), 1157–1166 (1978).
9. D. W. Sweeney and C. M. Vest, "Reconstruction of three-dimensional refractive index fields from multidirectional interferometric data," *Appl. Opt.* **12**(11), 2649–2664 (1973).
10. L. V. Kovalskii and V. K. Polanskii, "Application of the prism method for investigating transparent media with a refractive index gradient," *Opt. Spectrosc.* **20**, 408–409 (1966).
11. M. Miller and V. Malisek, "Study of the distribution of refractive index by the differential prism method," *Opt. Spectrosc.* **25**, 70–72 (1968).
12. G. Oster, M. Wasserman, and C. Zwerling, "Theoretical interpretation of moiré patterns," *J. Opt. Soc. Am.* **54**(2), 169–175 (1964).
13. Y. Nishijima and G. Oster, "Moiré patterns: their application to refractive index and refractive index gradient measurements," *J. Opt. Soc. Am.* **54**(1), 1–5 (1964).
14. J. Teichman, "Measurement of gradient index materials by beam deflection, displacement, or mode conversion," *Opt. Eng.* **52**(11), in press (2013).
15. G. Beliakov and S. Buckley, "Reconstruction of the refractive index profile of planar waveguides using ray tracing analysis," in *Optical Networking: Technologies, Traffic Engineering and Management: Conf. Proc.*, pp. 384–387, COIN/ACOFT, Melbourne (2003).

Di Lin received his BS degree in electrical engineering from the University of Minnesota in 2008. He is currently working toward his PhD degree in electrical engineering at the University of Minnesota. His principal research interests include light propagation in inhomogeneous materials, laser cavity design, and beam combining.

James R. Leger received his BS degree in applied physics from the California Institute of Technology, Pasadena, in 1974, and his PhD degree in electrical engineering (applied physics) from the University of California, San Diego, in 1980. He worked for the 3M Company until 1984, when he joined the Massachusetts Institute of Technology Lincoln laboratory, Lexington, as a research staff member. In 1991, he joined the faculty at the University of Minnesota, Minneapolis, where he is currently the Cymer professor of electrical and computer engineering and the Taylor distinguished professor. His principal research interests include laser design, applications of diffraction, and advanced imaging systems. He is a fellow of the Optical Society of America, the International Society for Optical Engineers, and the Institute of Electrical and Electronics Engineers.

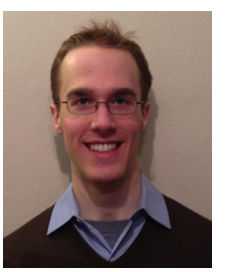

Mint Kunkel received his BA degree in physics from Carleton College in 2012. He is a research assistant to Professor Leger and is currently working toward his PhD degree in electrical engineering at the University of Minnesota. His main research interests include laser cavity design and optical signal processing.

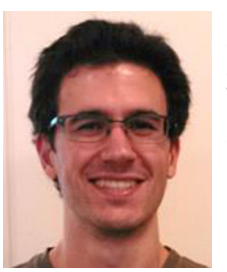

Peter McCarthy received his BS degree in optics from the University of Rochester in 2008. He is currently a PhD candidate at the Institute of Optics, University of Rochester, working in the research group of Professor Duncan Moore. His research interests include gradient-index metrology and optical system design.

Downloaded From: http://opticalengineering.spiedigitallibrary.org/ on 02/24/2014 Terms of Use: http://spiedl.org/terms